

Full-transparent zone plates for THz focusing

Hui Yin (尹慧)^{1,2}, Jiaqi Li (李佳奇)^{1,2}, Huawei Liang (梁华伟)^{1,2,*}, Min Zhang (张敏)^{1,2,**},
Hong Su (苏红)^{1,2}, and Ireng Ling Li (李玲)^{1,2}

¹Shenzhen Key Laboratory of Laser Engineering, Shenzhen University, Shenzhen 518060, China

²Guangdong Provincial Key Laboratory of Micro/Nano Optomechatronics Engineering, Shenzhen University, Shenzhen 518060, China

*Corresponding author: hwliang@szu.edu.cn; **corresponding author: zhangmin@szu.edu.cn

Received April 9, 2018; accepted June 6, 2018; posted online July 2, 2018

A full-transparent zone plate (FTZP), which can reuse the wave blocked in the focusing of the Fresnel zone plate (FZP), is proposed to improve the efficiency of terahertz (THz) focusing without aberration. We find that the substrate thickness of the FTZP has a great influence on the focusing intensity, which results from the Fabry–Perot effect. The focusing efficiency of FTZPs could be about twice as high as that of FZPs, but the widths of both focus spots are comparable with the wavelength. The experimental results are in good agreement with the simulation.

OCIS codes: 260.3090, 050.1940.
doi: 10.3788/COL201816.082601.

The terahertz (THz) wave, located between microwave and infrared frequency, is normally defined as the range from 0.1 to 10 THz. In recent years, THz technology has attracted extensive attention for its great application potential in many fields, such as sensing, imaging, and spectroscopy^[1–10]. THz focusing is a basic but very important technology. Parabolic mirrors, silicon lenses, and polyethylene lenses are conventional elements for THz focusing, but the accompanying aberration limits their applications to a certain extent.

In order to solve this problem, some kinds of diffractive THz elements have been proposed^[11–19]. Binary silicon lenses fabricated by means of ion etching could focus the THz wave effectively, but the fabrication required specialized equipment and is not widely available^[11]. Siemion *et al.* proposed a diffractive paper lens, which was made of the laser-cut thick paper, to focus the THz wave^[12]. Furlan *et al.* used a three-dimensional (3D) printed diffractive lens to obtain focusing at 0.625 THz^[13]. However, both the paper lens and the 3D printed lens are easy to deform when their diameters are large enough. Mendis *et al.* proposed an artificial dielectric lens made up of a parallel stack of 100 μm thick metal plates, which was capable of focusing a 2 cm diameter beam to a spot size of 4 mm at 0.17 THz^[14]. Recently, many researchers proposed to use metasurfaces to focus the THz wave, but the theoretical upper limit of monolayer metal wire metasurfaces based on the cross-polarization effect was only 25%^[15–17]. Multilayer metasurfaces could greatly improve the focusing efficiency, but the designing and fabricating become more difficult^[18–20].

The Fresnel zone plate (FZP) can also be used to obtain THz focusing without aberration, but the work efficiency is very low, because about half the incident THz wave is blocked. In order to improve the efficiency of THz focusing without aberration, we propose a full-transparent zone plate (FTZP), which can reuse the incident wave blocked

in the FZP focusing. The FTZP is obtained by mechanically machining a number of ring grooves on a quartz wafer, which is much easier to fabricate than the binary silicon lens, especially for longer wavelengths^[11]. The whole thickness of the quartz FTZP, which is not easy to deform, is smaller than the wavelength and also smaller than the 3D printed diffractive lens at the same wavelength^[13]. We theoretically and experimentally study the focusing characteristics of both FTZPs and FZPs at 0.14 THz, one of the atmospheric windows, and the experimental results are in good agreement with the simulation. In particular, we find that the substrate thickness of the FTZP has a great influence on the focusing intensity, which results from the Fabry–Perot effect. Compared with FZPs, both the peak intensity and the transmission efficiency of FTZPs increase a lot, but the widths of focus spots are still comparable with the wavelength. The advantages of high focusing efficiency, sub-wavelength thickness, non-deforming, and easy fabrication make the FTZP important in narrow-band THz wave imaging and sensing applications.

For the conventional FZP shown in Fig. 1(a), the focus length obeys the following relationship:

$$r_k^2 + f^2 = \left(f + k \cdot \frac{\lambda}{2}\right)^2, \quad (1)$$

where λ is the wavelength of the incident wave, k is the order number of the half-wave zone, and r_k is the corresponding outer radius of the half-wave zone. For FZP focusing, about half of the incident wave is blocked, which severely influences its work efficiency. In order to improve it, we propose an FTZP, as shown in Fig. 1(b), to focus the THz wave. The radii of half-wave zones in the FTZP are equal to the corresponding ones of the FZP. The materials in the even ($k = 2, 4, 6, \dots$) and odd ($k = 1, 3, 5, \dots$) half-wave zones are air and another dielectric, respectively,

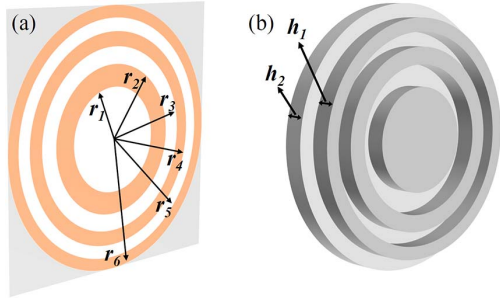


Fig. 1. Schematics of the (a) FZP and (b) FTZP.

and they can also be exchanged. When the THz wave is incident to the FTZP, the optical path difference caused by the two different dielectrics is $\delta = (n_2 - n_1)h_1$, where n_1 and n_2 are refractive indices of air and the other dielectric, respectively, and h_1 is the groove depth. The interference enhancement of the transmission THz wave can be achieved when $\delta = (n + 1/2)\lambda$, and we adopt $n = 0$ to reduce the intrinsic absorption loss of the dielectric.

Here, our studies focus on the frequency $f_0 = 0.14$ THz, which is one of the atmospheric windows of the THz wave. Three FTZPs with different focal lengths $f = 4, 5$, and 6 cm, respectively, are studied, and all of the FTZPs have six half-wave bands. According to Eq. (1), the most outer radii ($k = 6$) of the three FTZPs are 2.36, 2.62, and 2.85 cm, respectively. The quartz ($n_2 = 2.1$) with low intrinsic loss is adopted as the dielectric material, and the substrate is also quartz for the convenience of fabricating. When the THz wave is incident to the FTZP, it will form the Fabry–Pérot interference in the quartz plate, so the substrate thickness h_2 has a great influence on the transmission efficiency. Supposing the reflectivity at the air/quartz interface is ρ , when the incident angle is 0° , the ratio of transmission intensity to the incident one can be written as^[21]

$$\frac{I_t}{I_i} = \frac{1}{1 + \frac{4\rho}{(1-\rho)^2} \sin^2\left(\frac{\varphi}{2}\right)}, \quad (2)$$

where $\varphi = 4\pi n_2 h_2 / \lambda$. Based on Eq. (2), we obtain the dependence of the transmission rate on the thickness of a quartz slab, as shown by the dashed line in Fig. 2. We further calculate the varying of the peak intensity at the focal point with the substrate thickness by using COMSOL software for the focal length $f = 5$ cm, as shown by the point solid line in Fig. 2. The transmission characteristics for $f = 4$ and 6 cm are very similar to that for $f = 5$ cm. We can observe that there are three peaks in each line, but there is some offset between the corresponding peaks in the two lines. The offset mainly results from the difference of the quartz thickness between the even and odd half-wave zones, which is different from the quartz slab with the same thickness at different positions. In addition, due to the intrinsic absorption loss of the

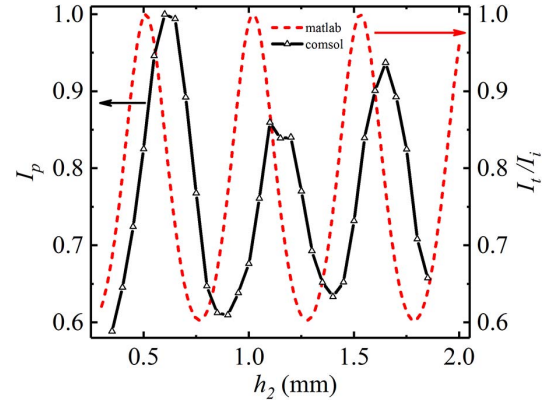


Fig. 2. Dependence of the THz wave transmission on the substrate thickness. The peak intensity at the focal point for the focal length $f = 5$ cm is shown by the point solid line, and the transmission rate is shown by the dashed line.

quartz and the influence of the edges of half-wave zones, the intensities of the second and third peaks at the focus points are lower than that of the first one. In the subsequent simulation and experiment, the thickness of the quartz substrate is adopted as $h_2 = 0.65$ mm, which is the smallest one corresponding to the transmission peaks. In order to study the work characteristics of the FTZP, we calculate the focusing of the THz wave along the propagation direction for $f = 4, 5$, and 6 cm, as shown in Figs. 3(a)–3(c). The corresponding focusing of the FZP is also simulated for comparison, as shown in Figs. 3(d)–3(f). We can observe that both the FTZP and FZP focus the THz wave to the predesigned focal planes. The peak values of FTZPs with $f = 4, 5$, and 6 cm are 2.3, 2.4, and 2.2 times as high as that of the FZPs, respectively. For a given FTZP with the focal length $f = 5$ cm for $f_0 = 0.14$ THz, when the frequency f_0 changes from 0.12 to 0.15 THz, the focal length will gradually increase, which is consistent with Eq. (1). Therefore, the FTZP can focus the THz wave in a wide band range, but it is important to pay attention to the change of the focal length.

The focusing experiment setup is shown in Fig. 4(a). An impact ionization avalanche transit-time (IMPATT) diode working at a frequency of 0.14 THz is employed as the THz source. The emitted THz wave is collimated by a commercial lens and then focused by the fabricated FTZP shown in Fig. 4(b), which is obtained by mechanically machining a number of ring grooves on a quartz wafer. The focused THz wave is collected at the designed focal planes by a Pyrocam III beam profiling camera. The focus spots corresponding to the focal lengths $f = 4, 5$, and 6 cm are shown in Figs. 5(a), 5(b), and 5(c), respectively. We further focus the THz wave by using FZPs, which are obtained by coating some annular copper films on the polyimide substrate with 100 μm thickness, for comparison, and the intensity distributions on the focal planes for $f = 4, 5$, and 6 cm are shown in Figs. 5(d), 5(e), and 5(f), respectively. The full widths at half-maximum (FWHMs)

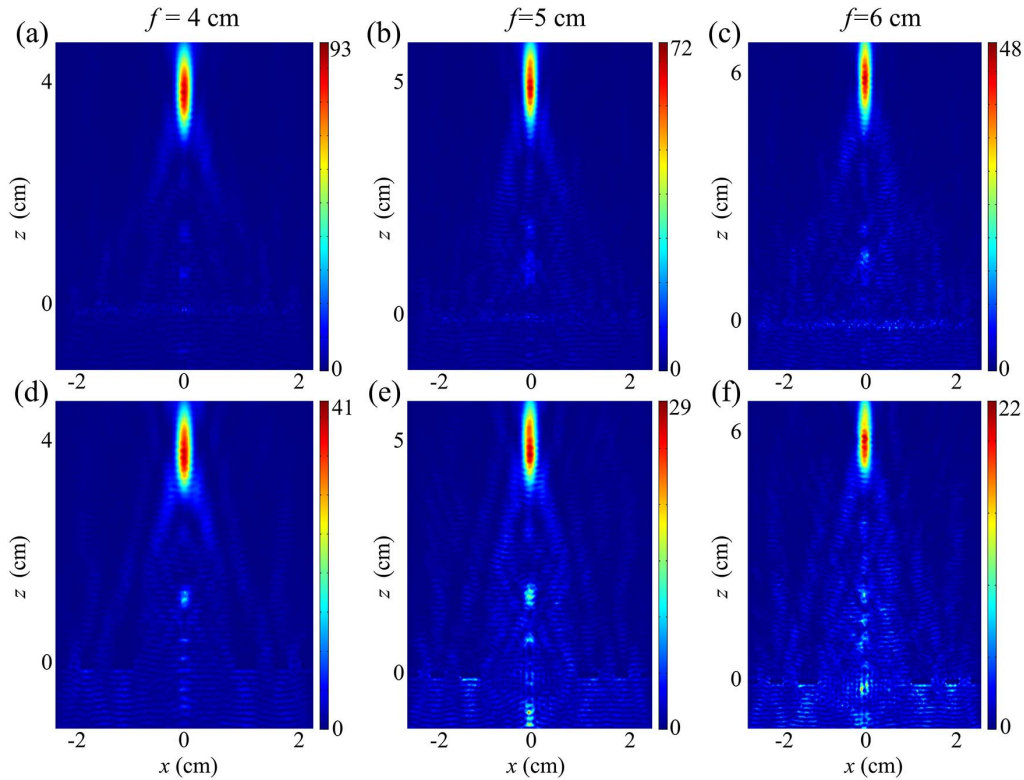


Fig. 3. THz field intensities on the longitudinal sections for the focusing of FTZPs: (a) $f = 4$ cm, (b) $f = 5$ cm, (c) $f = 6$ cm; and FZPs: (d) $f = 4$ cm, (e) $f = 5$ cm, (f) $f = 6$ cm.

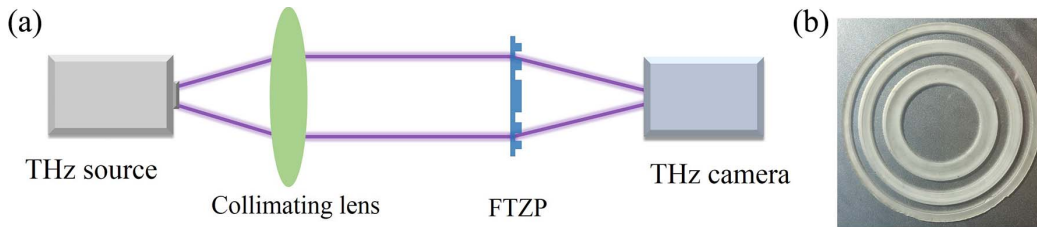


Fig. 4. (a) Experimental setup for the FTZP focusing. (b) FTZP sample.

of focus spots corresponding to FTZPs with $f = 4$, 5, and 6 cm are 2.3, 2.3, and 2.6 mm, respectively, which are 28%, 42%, and 26% smaller than those for FZPs. Moreover, the peak field intensities of focus spots for FTZPs with $f = 4$, 5, and 6 cm are 2, 2.8, and 1.9 times, respectively, as large as those for FZPs. The experimental results agree well with the previous simulation.

In order to obtain the focusing efficiency, we calculate the THz power by integration of the data obtained from the THz camera. Then, by replacing the FTZP with a gold-plated parabolic mirror in Fig. 4(a), we collect the THz wave at the focal plane with the camera and obtain the total incident power by the integration of the recorded data. The focusing efficiencies of FTZPs, defined as the ratio of the THz power at the focal plane to the total incident power, are 29%, 38%, and 38%, respectively, for $f = 4$, 5, and 6 cm, which are 1.9, 2.1, and 1.7 times as high as those for FZPs. The focusing efficiencies are

also higher than the theoretical upper limit of monolayer metal wire metasurfaces based on the cross-polarization effect^[15–17].

We propose an FTZP, which can reuse the wave blocked in the FZP focusing, to improve the efficiency of THz focusing without aberration. According to the simulated results obtained by using COMSOL, the substrate thickness of the FTZP greatly affects the focusing intensity of the THz wave, which results from the Fabry–Perot effect. We further theoretically and experimentally study the focusing characteristics of both FTZPs and FZPs with the focal lengths $f = 4$, 5, and 6 cm. The study results show that both the peak intensity and the transmission efficiency of FTZPs are much higher than those of FZPs, and, at the same time, the widths of THz focus spots are still comparable with the wavelength, which are very important for many THz applications, such as narrow-band imaging and sensing.

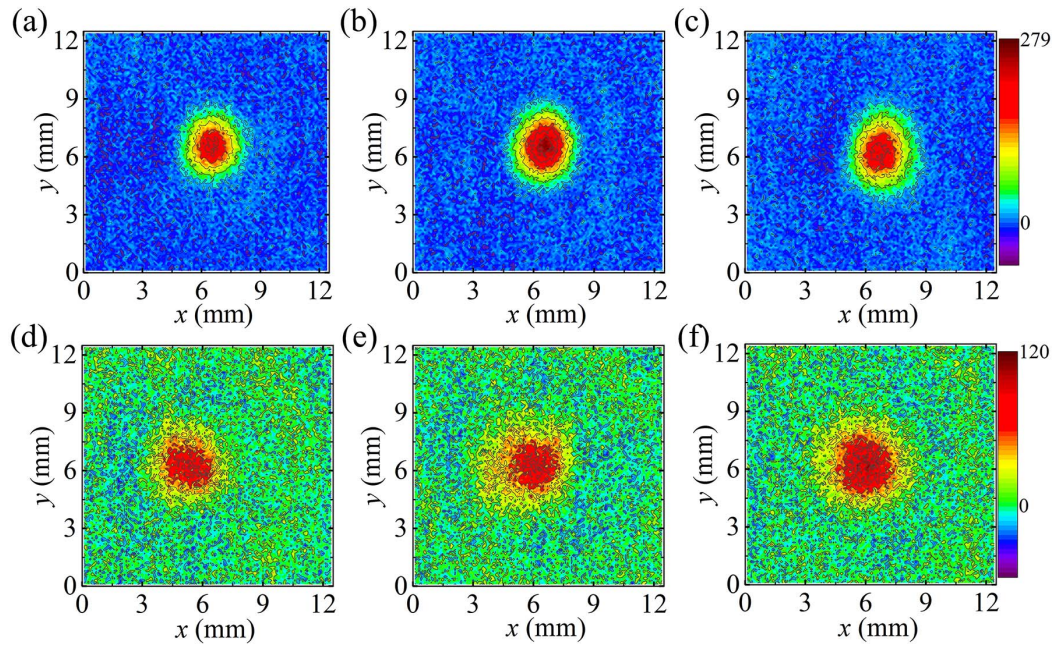


Fig. 5. Measured THz intensity distributions on the focal planes for FTZPs: (a) $f = 4$ cm, (b) $f = 5$ cm, (c) $f = 6$ cm; and FZPs: (d) $f = 4$ cm, (e) $f = 5$ cm, (f) $f = 6$ cm.

This work was supported in part by the National Natural Science Foundation of China (No. 61405124), the Fund Project for Shenzhen Fundamental Research Programme, China (No. JCYJ20170818143652693), and the Major Science and Technology Project of Guangdong Province (No. 2014B010131006).

References

1. D. Mittleman, *Sensing with Terahertz Radiation* (Springer, 2003).
2. S. Wang and X. Zhang, *J. Phys. D Appl. Phys.* **37**, R1 (2004).
3. K. Kawase, Y. Ogawa, Y. Watanabe, and H. Inoue, *Opt. Express* **11**, 2549 (2003).
4. M. J. Fitch and R. Osiander, *Johns Hopkins APL Tech. Dig.* **25**, 348 (2004).
5. J. Yang, G. Lin, Y. Niu, Y. Qi, F. Zhou, and S. Gong, *Chin. Opt. Lett.* **14**, 072401 (2016).
6. L. Chen, N. Xu, L. Singh, T. Cui, R. Singh, Y. Zhu, and W. Zhang, *Adv. Opt. Mater.* **5**, 1600960 (2017).
7. L. Chen, Y. Wei, X. Zang, Y. Zhu, and S. Zhuang, *Sci. Rep.* **6**, 22027 (2016).
8. Q. Wang, Q. Xu, X. Zhang, C. Tian, Y. Xu, J. Gu, Z. Tian, C. Ouyang, X. Zhang, J. Han, and W. Zhang, *ACS Photon.* **5**, 599 (2018).
9. L. Luo, K. Wang, C. Ge, K. Guo, F. Shen, Z. Yin, and Z. Guo, *Photon. Res.* **5**, 604 (2017).
10. X. Xu, Y. Wu, T. He, Y. Li, F. Hu, H. Liang, C. Yang, and H. Zhong, *Chin. Opt. Lett.* **15**, 111703 (2017).
11. S. Wang, T. Yuan, E. D. Walsby, R. J. Blaikie, S. M. Durbin, D. R. Cumming, J. Xu, and X. C. Zhang, *Opt. Lett.* **27**, 1183 (2002).
12. A. Siemion, A. Siemion, M. Makowski, J. Suszek, J. Bomba, A. Czerwiński, F. Garet, J. L. Coutaz, and M. Sypek, *Opt. Lett.* **37**, 4320 (2012).
13. W. D. Furlan, V. Ferrando, J. A. Monsoriu, P. Zagrajek, E. Czerwińska, and M. Szustakowski, *Opt. Lett.* **41**, 1748 (2016).
14. R. Mendis, M. Nagai, Y. Wang, N. Karl, and D. M. Mittleman, *Sci. Rep.* **6**, 23023 (2016).
15. Q. Wang, X. Zhang, Y. Xu, Z. Tian, J. Gu, W. Yue, S. Zhang, J. Han, and W. Zhang, *Adv. Opt. Mater.* **3**, 779 (2015).
16. X. Y. Jiang, J. S. Ye, J. W. He, X. K. Wang, D. Hu, S. F. Feng, Q. Kan, and Y. Zhang, *Opt. Express* **21**, 30030 (2013).
17. L. Zhang, M. Zhang, and H. Liang, *Adv. Opt. Mater.* **5**, 1700486 (2017).
18. C. C. Chang, D. Headland, D. Abbott, W. Withayachumnankul, and H. T. Chen, *Opt. Lett.* **42**, 1867 (2017).
19. H. Zhao, X. Wang, J. He, J. Guo, J. Ye, K. Qiang, and Z. Yan, *Sci. Rep.* **7**, 17882 (2017).
20. X. J. Shang, X. Zhai, L. L. Wang, M. D. He, Q. Li, X. Luo, and H. G. Duan, *Appl. Phys. Express* **10**, 052602 (2017).
21. A. Yariv and P. Yeh, *Optical Electronics in Modern Communications* (Oxford University, 2006).